Thermal Stability and Ordering Study of Long- and Short-Alkyl Chain Phosphonic Acid Multilayers

ARTICLE *in* LANGMUIR · SEPTEMBER 2012

Impact Factor: 4.46 · DOI: 10.1021/la303087t · Source: PubMed

8 AUTHORS, INCLUDING:

Matheus Josué de Souza Matos
Universidade Federal de Ouro Preto
14 PUBLICATIONS **83** CITATIONS
SEE PROFILE

Giselle Fontes
National Institute of Metrology, Quality and …
11 PUBLICATIONS **96** CITATIONS
SEE PROFILE

Carlos Alberto Perez
Centro Nacional de Pesquisa em Energia e M…
87 PUBLICATIONS **624** CITATIONS
SEE PROFILE

Bernardo R A Neves
Federal University of Minas Gerais
82 PUBLICATIONS **1,182** CITATIONS
SEE PROFILE

Langmuir

Article

pubs.acs.org/Langmuir

Thermal Stability and Ordering Study of Long- and Short-Alkyl Chain Phosphonic Acid Multilayers

Muriel de Pauli, [†,‡] Mariana de Castro Prado,[§] Matheus Josue Souza Matos,[§] Giselle Nogueira Fontes,[∥] Carlos Alberto Perez, [†] Mario Sergio Carvalho Mazzoni,[§] Bernardo Ruegger Almeida Neves,[§] and Angelo Malachias[§,*]

[†]Laboratório Nacional de Luz Síncrotron, Caixa Postal, 6192 - CEP 13083-970, Campinas, SP, Brazil

[‡]Instituto de Física Gleb Wataghin, Universidade Estadual de Campinas, CEP 13083-859, Campinas, SP, Brazil

[§]Depto. de Física, ICEx, Universidade Federal de Minas Gerais, Av. Antonio Carlos, 6627 - CEP 30123-970, Belo Horizonte, MG, Brazil

[∥]Divisão de Metrologia de Materiais, Instituto Nacional de Metrologia, Normalização e Qualidade Industrial (INMETRO) - CEP 25250-020, Duque de Caxias, RJ, Brazil

ABSTRACT: Long-range order evolution of self-assembled phosphonic acid multilayers as a function of temperature is studied here for two molecules with different alkyl chain length. By using synchrotron conventional diffraction, distinct order configurations are retrieved on phosphonic acid multilayers and their thermodynamic behavior monitored by energy-dispersive diffraction. This later technique allows us to observe the system behavior near order−disorder temperatures, as well as to determine the most stable configurations in the range from room temperature up to 120 °C. Planar order is also addressed by wide-angle X-ray scattering (WAXS) transmission experiments. Order parameter phase diagrams are built based on the experimental results, showing the dominant configuration at each temperature. The multilayer molecular long-range order retrieved from the experiments is corroborated by first principles calculations based on the Density Functional Theory. The bulk configurations depicted in this work are produced by molecule−molecule interactions and allow for future comparisons with the behavior of ordered molecules in few-monolayers configurations, commonly used in organic devices, where the presence of surfaces and interfaces strongly affects the molecule packing.

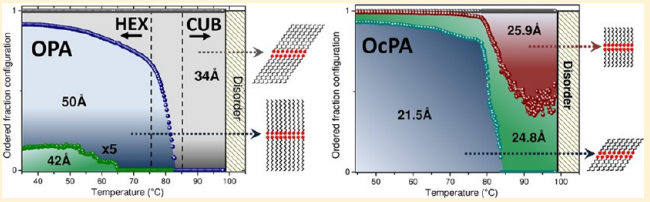

INTRODUCTION

Amphiphilic molecules have been intensively studied in the past decades due to their wide range of applications in many areas. Their self-assembly capabilities provide the possibility of fabrication of long-range ordered structures with good coverage and layer thickness control. Surfaces modifications and functionalization can be obtained by the coating with specific organic molecules[1−3] and some of these systems have been used in the fabrication of optical[4] and electronic devices.[5−7] Phosphonic acids monolayers and few-layer structural behavior have been intensively studied[8−10] and are crucial for state-of-the-art devices.[5] However, the configurations obtained when the molecules are in contact with surfaces and interfaces can be strongly affected by chemical interactions between molecules and their hosting substrates. As the number of monolayers (or bilayers) in a given system increases, the molecule−molecule interactions become extremely relevant. Knowing whether such interactions can compete or overcome the molecule−surface interactions is crucial since the precise control of their structural packing may influence device properties such as leakage currents and working temperature range.

Phase transition,[11,12] structural, and morphological studies[13−15] have been performed in a plethora of organic systems. Nevertheless, the detailed evolution of structural organization as a function of the temperature requires a combination of techniques and, therefore, has not been much explored in phosphonic acids, although the influence of alkyl chain length on in-plane long-range order had been addressed for phosphonic acid monolayers at room temperature.[16] In the present work, we report detailed configuration and thermal stability analysis of multilayers obtained from two different phosphonic molecules, one with a longer alkyl chain—Octadecylphosphonic acid (OPA) $[CH_3(CH_2)_{17}PO(OH)_2]$—and a shorter molecule − Octylphosphonic acid (OcPA) $[CH_3(CH_2)_7PO(OH)_2]$ both of interest for device fabrication or as a model system for understanding similar molecules.[5] Studying phosphonic acid multilayers with a large number of mono- or bilayers offers the possibility of observing stable configurations that are related to pure molecular interactions. Such information is crucial even to understand systems with few layers where the resulting molecule packing has weak influence from the substrate and can be simply ascribed to bulk

Received: January 3, 2012
Revised: September 20, 2012

   dx.doi.org/10.1021/la303087t | *Langmuir* XXXX, XXX, XXX−XXX

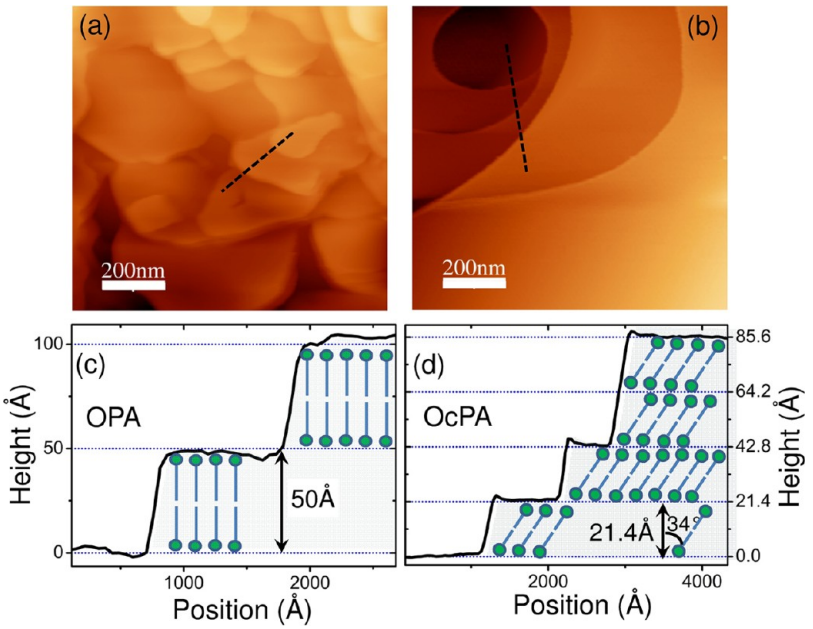

Figure 1. AFM images of (a) OPA and (b) OcPA multilayers at room temperature. The full height range (z color scale) is 900 Å for (a) and 150 Å for (b). Surface height profile showing the presence of ordered (c) OPA bilayers stacked perpendicularly to the substrate and (d) OcPA bilayers ordered forming an angle of 34° with respect to the surface normal.

configurations. The thermal stability of observed configurations in multilayers reveal if different packings can coexist, if there is the possibility of reorganization among distinct configurations, and which molecular packing is more stable and can withstand local or global energy fluctuations.

The formation of phosphonic acid multilayers has been observed previously by atomic force microscopy (AFM)[17] as well as by X-ray diffraction.[13] AFM is usually employed preliminarily to other analysis since it directly provides information about the surface topography, evidencing the ordering of the amphiphilic molecules in the self-ordered stacking. AFM measurements performed in OPA bilayers evidenced that the surface order configuration of molecules strongly changes as a function of the temperature.[18] However, the configuration of layers that lie underneath the surface cannot be probed via AFM and methods that directly assess their structure must be employed.

Angular-resolved X-ray diffraction (AR-XRD) and energy dispersive diffraction (EDD) were therefore used to address the lamellar order of multilayers of OPA and OcPA molecules. AR-XRD measurements provide excellent reciprocal space resolution and thus are performed to infer the lamellar configuration in self-assembled multilayers. However, in systems with rapid structural changes such as phase transitions or chemical reactions, the angular resolution may not be a crucial parameter. The EDD technique provides then short time of data acquisition allowing the precise monitoring of the changes in the periodicity configuration or reaction time.[19−22] Thus, EDD was used here to investigate changes in periodicity on OPA and OcPA multilayers as a function of the temperature. Finally, the in-plane configuration of OPA multilayers was studied by small and wide angle X-ray scattering (SAXS/WAXS). The stability of the molecular configurations observed was investigated by Density Functional Theory simulations for the observed bulk packing geometries.

Combining the experimental techniques of this work, we mapped out the presence of different periodicities in the OPA and OcPA multilayers, showing the possibility of distinct stacking order and its temperature dependence. With the information about the lamellar and in-plane configurations, it was possible to construct an order parameter phase diagram to OPA and OcPA systems.

METHODS

The phosphonic acids studied here are amphiphilic molecules, consisting of a hydrophilic head and a hydrophobic tail. The main difference between the OPA and OcPA molecules is the alkyl chain length—implying molecule lengths for OPA and OcPA of 25 and 13 Å, respectively. Samples were prepared using a 5 mM concentrated solution of OPA (OcPA) molecules diluted in ethanol. The solution was spread coated in silicon (100) substrates with native SiO_2 layers (~25-Å thick) using a micrometric pipet, in steps of 1 μL. The solvent was then evaporated slowly by an ultrapure nitrogen (99.99%) gas circulation. For OPA samples, the amounts of material deposited for AR-XRD, EDD, and AFM measurements were 4, 2, and 1 μL, respectively. For OcPA samples, 9 μL were used for AR-XRD measurements, while 4 μL were used for EDD measurements and 1 μL was used for AFM images. According to previous works,[13,21,23] this procedure leads to the formation of several stacked OPA or OcPA bilayers. AR-XRD measurements performed previously to EDD measurements in all samples have not shown variations in the relative volume fraction of the different ordered periodicities found in this work with respect to the total amount of deposited phosphonic acids. The initial characterization of the samples was performed by tapping mode AFM, employed to ensure the existence of OPA and OcPA bilayers stacked as described in previous works.[4,13] A Veeco Nanoscope IIIa from the MTA group at the Brazilian Synchrotron Light Laboratory (LNLS) was used.

AR-XRD and EDD measurements were performed in the XRD2 and XRF beamlines, respectively, of the LNLS. Both beamlines are placed in bending magnet sources. The XRD2 beamline is equipped with a cylindrically bent Rh-coated mirror and a sagital Si(111) double crystal monochromator, which are used to focus the monochromatic X-ray beam to a spot of 2 mm (horizontal) × 0.7 mm (vertical) in the experimental hutch, equipped with a 4 + 2 circle diffractometer. AR-XRD measurements were performed at room temperature and with monochromatic photons with energy fixed at E = 8 KeV.

dx.doi.org/10.1021/la303087t | Langmuir XXXX, XXX, XXX−XXX

The experimental setup built to perform EDD measurements consists of a chamber equipped with a sample rotation axis (θ), a temperature stage, capable of reaching 300 °C under inert atmosphere (N_2) and a 2θ-arm, with 1 m length, that holds an energy sensitive detector.[21] For the measurements shown here, a Ketek Si-drift detector with 150 eV energy resolution and maximum count rate of 10^5 counts per second was used. The setup is installed in the XRF beamline, in which the optics allow for using the white (polycromatic) beam from the bending magnet source. The beam size at the sample position was limited to 200 × 200 μm by slits.

Small angle X-ray scattering (SAXS) and wide angle X-ray scattering (WAXS) measurements were performed simultaneously using the SAXS1 beamline at LNLS. The measurements shown here were performed in transmission mode with E = 9 KeV. A Pilatus 100k detector from Dectris was used for WAXS measurements, with a fixed distance detector-sample of 117 mm, covering a scattering angle range that spans from 7° to 42°. For SAXS measurements, a Pilatus 300k was placed 1 m away from the sample. The curves shown here were obtained using the cake procedure from the Fit2D software.[24] For SAXS/WAXS measurements, the solution with phosphonic acid molecules was dropped on thin mica substrates. Since the scattering cross section of organic materials is reduced, the total amount of material in each sample needed to be larger than that used in diffraction measurements (about 50 μL).

First principles calculations based on the Density Functional Theory (DFT)[25,26] are known to give good results for ground state properties. Therefore, we use this formalism to investigate the relationship between structural and energetic properties of the different crystalline phases adopted by OPA and OcPA phosphonic acids. Our DFT calculations[25,26] are based on the SIESTA implementation,[27] which makes use of an exchange-correlation functional that takes into account the van der Waals interactions in a self-consistent way by means of an efficient algorithm developed by Román-Pérez and Soler.[28,29] We employ norm-conserving Troullier−Martins pseudopotentials[30] in the Kleinman−Bylander factorized form,[31] and a double-ζ basis set composed of finite-range numerical atomic pseudofunctions enhanced with polarization orbitals (DZP basis set). A real space was used with a cutoff of 350 Ry. All geometries were optimized so that the maximum force component on any atom was less than 10 meV/atom. Different schemes of relaxation were employed, keeping the non-diagonal elements of the stress tensor fixed (to avoid in plane distortions), allowing them to change together with the coordinates, or keeping the entire cell fixed. In all of them, no constraints were imposed on atomic positions, which were kept free to change according to the forces.

RESULTS

Atomic force microscopy images of OPA and OcPA multilayers at room temperature are shown in Figure 1, parts (a) and (b), respectively. Both images have an area of 1 × 1 μm. Figure 1, parts (c) and (d), shows height profiles extracted along the dashed lines in the AFM images. In Figure 1(c), one observes topography steps with about 50 Å periodicity, evidencing the presence of stacked OPA bilayers ordered perpendicularly to the substrate. Previous works observed a 34 Å stacking periodicity, denoting that tilted bilayers with an angle of 47° with respect to the surface normal are also formed below the surface.[13] In the Figure 1(d), we observe the OcPA bilayer profile showing a periodicity of 21.4 Å. Since for this molecule the expected periodicity for a bilayer oriented perpendicularly to the substrate is of 26 Å, the topography steps indicate that surface molecules are tilted by 34° with respect to the surface normal at room temperature.

In-situ AFM heating was also used to evidence the surface morphology for few fixed temperatures. Figure 2 shows 2 × 2 μm AFM images and selected profiles (insets) of OPA and OcPA multilayers at different temperatures. Fixing the temperature at 80 °C for 1 h one can still observe the stacking of ~50 Å steps at the OPA multilayers, as shown in Figure 2(a) (see also ref 18). For higher temperatures such as 95 °C (and 1 h thermalization), shown in Figure 2(b), large disordered droplets are observed. At this temperature, a single bilayer step remains covering part of the surface. OcPA multilayers—seen in Figure 2(c)—show disordered surface profiles at relatively lower temperatures if compared to OPA, such as 60 °C, with

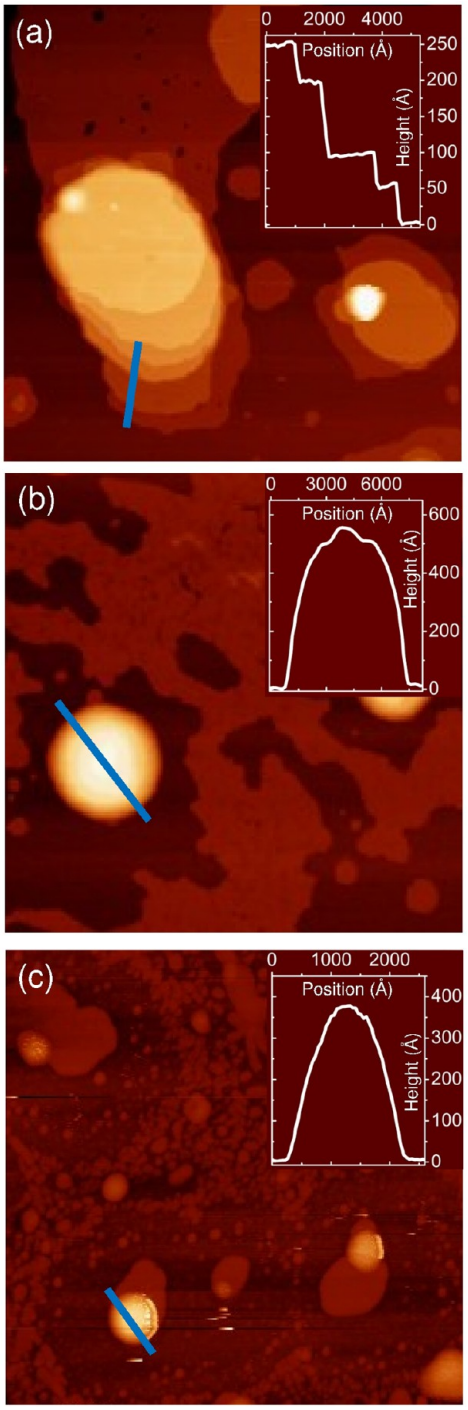

Figure 2. Two μm × 2 μm AFM images and selected profiles (insets) of OPA multilayers heated in situ at 80 °C (a) and 95 °C (b) and OcPA multilayers heated at 60 °C (c). A minimum thermalization time of 30 min was used for each measurement. The insets show height profiles along directions indicated by solid lines.

dx.doi.org/10.1021/la303087t | Langmuir XXXX, XXX, XXX−XXX

large and small droplets that could be initially ascribed to disordered molecules.

One must notice that AFM measurements provide information only about the sample surface restricting the multilayer analysis. The absence of lamellar order in OPA and OcPA molecules at the surfaces of Figure 2, parts (b) and (c), is nevertheless insufficient to rule out the possibility of existence of ordered configurations inside the observed droplets. Angular-resolved X-ray diffraction was then used to obtain information about the lamellar configuration established in multilayers of the two studied molecules. Figure 3, parts (a) and (b), shows

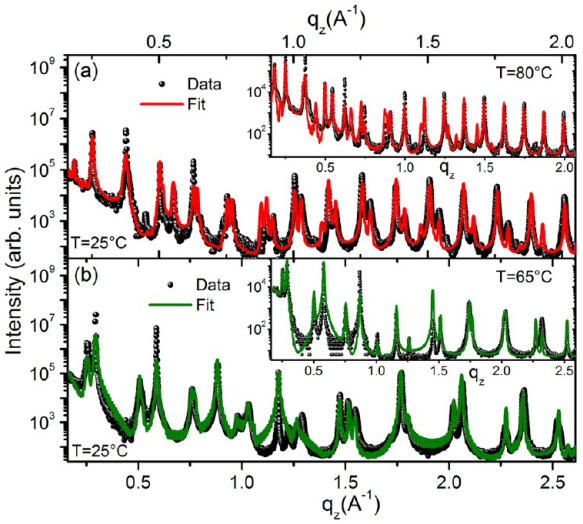

Figure 3. AR-XRD measurements at room temperature in (a) OPA and (b) OcPA self-assembled multilayers. Theoretical fits using the kinematical model described in the text are shown as solid lines. Insets in each figure show data and fits for higher temperatures (80 °C for OPA and 65 °C for OcPA).

AR-XRD measurements on OPA and OcPA multilayers, respectively, at room temperature. The diffraction intensity is shown as a function of the longitudinal momentum transfer vector, $q_z = (4\pi/\lambda)\sin(2\theta/2)$. In this representation, the Δq_z spacing between peaks is larger for the OcPA multilayers, denoting shorter periodicities with respect to OPA multilayers. Different peak-to-peak Δq_z intervals are observed, evidencing the presence of distinct periodicities in the same sample. Therefore, in order to fit the AR-XRD data, it is necessary to consider the contribution for the diffracted intensity of more than a single lamellar configuration.

Theoretical fits using a kinematical model were performed for the AR-XRD data to obtain structural information such as multilayer periodicity, roughness, correlation lengths and number of layers present in the sample.[32] The simulated scattered intensity represented by the solid lines in Figure 3, parts (a) and (b) is obtained as follows:

$$I(q_z) = \sum_{n=1}^{n} \alpha_n \left| \sum_{m=1}^{Nl} \sum_{j=1}^{Na} f_j \exp(iq(r_j + mD_n)) \right|^2 \frac{\exp(-(\sigma q_z)^2)}{q_z^2} \quad (1)$$

where Na is the number of atoms inside each bilayer, r_j is the position of the jth atom in the bilayer, Nl accounts for the number of bilayers comprising the coherently ordered domain with a given configuration, D is the thickness of a bilayer and σ is the mean interface roughness between the organic bilayers within the structure (acting as a static Debye−Waller attenuation factor). For tilted bilayers, r_j and D will represent the projection of an atom position and of the bilayer periodicity, respectively, in the z direction for a given tilt angle γ. The n index from the outermost summation in eq 1 is used to account for different bilayer periodicities. The final intensity in this model is therefore given by the incoherent sum of intensities for a few coexisting bilayer periodicities, each with a relative volume fraction α_n (with $\Sigma_n[\alpha_n] = 1$).

The best theoretical fits obtained for the AR-XRD data of the OPA multilayer at room temperature are represented by the solid line in Figure 3(a). Three lamellar periodicities were observed in the same sample at room temperature, as depicted in Table 1. Such distinct periodicities are directly related to

Table 1. Lamellar Periodicities Observed in OPA and OcPA Multilayers at Room Temperature by AR-XRD Measurements[a]

molecule	OPA	OcPA
$d1$ (Å)	50.0 (1)	26.9 (1)
tilt (degrees)	0	5°
$d2$ (Å)	48.9 (1)	24.8 (1)
tilt (degrees)	12°	17°
$d3$ (Å)	34.0 (1)	21.5 (1)
tilt (degrees)	47°	34°

[a]Tilt angles with respect to the surface normal are also provided.

different tilt angles of ordered molecules. The periodicity d1 represents a straight configuration, while $d2$ and $d3$ are related to tilted bilayers. The relative volume fractions of each periodicity in OPA multilayers were found to be $\alpha_1 = 0.890(3)$, $\alpha_2 = 0.050(1)$, and $\alpha_3 = 0.060(1)$. A similar coexistence of three distinct lamellar configurations was observed in OcPA multilayers at room temperature and the best fit (solid line) to the experimental data is shown in Figure 3(b), while the lamellar periodicities are listed in the Table 1. Relative volume fractions retrieved from OcPA multilayers were $\alpha_1 = 0.008(1)$, $\alpha_2 = 0.062(1)$ and $\alpha_3 = 0.930(3)$. For all fits, the narrow peaks observed require that the number of stacked bilayers of each family—Nl in eq 1—had to be of the order of 30, which may be limited by the X-ray coherence length given by the setup. This evidences that dealing with bulk-like multilayer systems, and the structural behavior of phosphonic acid molecules will depend exclusively on molecule−molecule interactions. Narrow diffraction peaks are still observed at higher temperatures as seen in the insets of Figure 3, parts (a) and (b), performed at 80 °C for OPA and 65 °C for OcPA, respectively. The observed peaks are still simulated assuming a large number of stacked bilayers, showing that bulk states remain dominant in both systems at these temperatures.

Although AR-XRD measurements provide excellent reciprocal space resolution, its efficiency to produce results in limited time frames is inherently constrained by the movements of angular stages in a diffractometer. A full measurement of the reciprocal space range, where the peaks of interest are located, takes about 1 h in a bending magnet synchrotron source, and performing a temperature ramp with large steps (about 10 °C/step) can induce structural transitions out of thermal equilibrium. It is therefore unfeasible to perform a large set of measurements for several temperatures (small temperatures

dx.doi.org/10.1021/la303087t | Langmuir XXXX, XXX, XXX−XXX

steps). In systems where the acquisition time is a crucial parameter and the structure is previously known, energy dispersive diffraction (EDD) can be performed to allow the acquisition of a denser data set.[21]

In order to provide a detailed plot of temperature evolution in our systems, EDD measurements were performed in OPA and OcPA multilayers. In Figure 4, we show selected snapshots

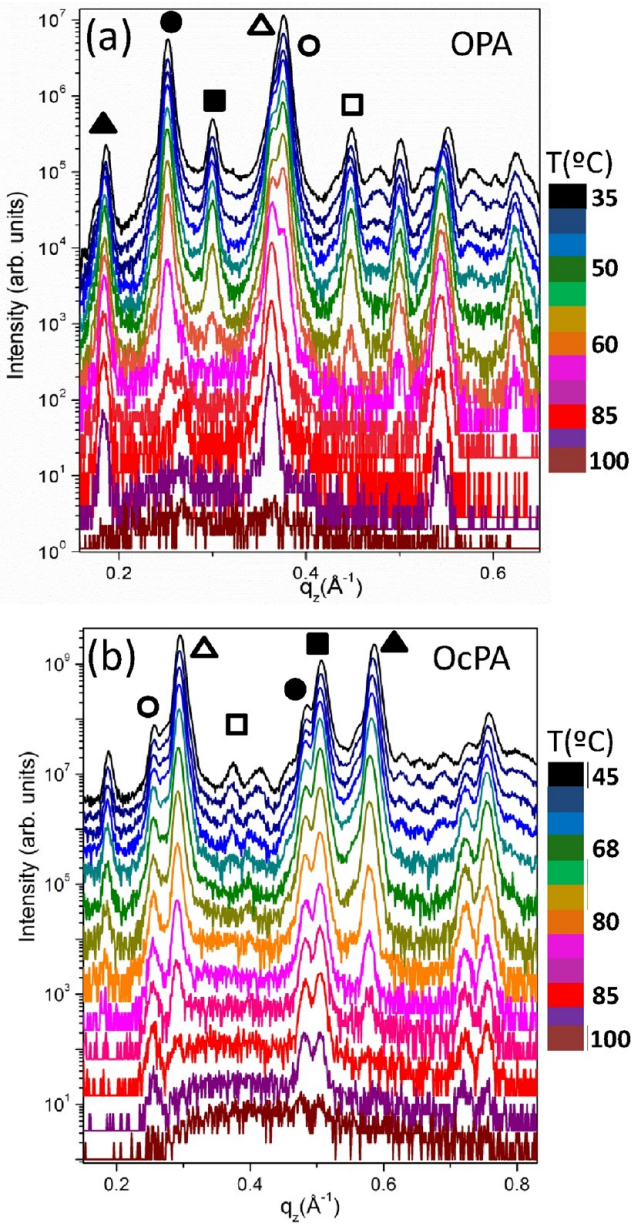

Figure 4. Selected snapshots of EDD measurements from (a) OPA and (b) OcPA multilayers. Diffraction peaks related to each configuration depicted in Table 2 are indentified by symbols. Solid symbols refer to peaks used for the area analysis of Figure 5. The curves were displaced for better visualization.

corresponding to different temperatures for both systems, depicting the modifications in the diffraction peaks configuration as the temperature increases. While some peaks disappear, others become relatively more significant, as explained in the following paragraphs.

Figure 4(a) shows selected EDD measurements in OPA multilayers. The measurements were performed with temperature steps of 0.3 °C, from room temperature (25 °C) to 103 °C (thus 260 snapshots). Since the temperature is increased in small steps, the heating process is near thermal equilibrium, allowing for quantitative description of the system in each state. The sample was kept under nitrogen atmosphere, with the scattering condition fixed at $\theta = 2.5°$, $2\theta = 5°$ and acquisition time of 50 s per temperature and thermalization intervals of 60 s between temperature steps. Three different periodicities are observed at room temperature, and are listed in Table 2. The

Table 2. Lamellar Periodicities Observed from OPA and OcPA Multilayers at Room Temperature by EDD Measurements[a]

molecule	OPA	OcPA
$d1$(Å) (●)	50.0 (6)	25.9 (6)
tilt (degrees)	0	5°
T_{1c} (°C)	83.1	98.6
$d2$ (Å) (■)	42.0 (6)	24.8 (6)
tilt (degrees)	33°	17°
T_{2c}(°C)	65.1	98.6
$d3$(Å) (▲)	34.0 (6)	21.5 (6)
tilt (degrees)	47°	34°
T_{3c} (°C)	98.3	83.9

[a]The symbols used to denote each periodicity are shown as peak labels in Figure 4. Molecule tilts for each configuration and order-disorder critical temperatures are also listed.

diffraction peak at $q_z = 0.300$ Å^{-1} is related to a 42-Å periodicity, and marked with a square in Figure 4(a). Such periodicity vanishes around 70 °C and was not observed by AR-XRD measurements most probably because the amount of ordered molecules within this configuration is minoritary and cannot be detected by conventional diffraction. However, the tilted periodicity of 48.9 Å detected by AR-XRD is not observed here due to the large lattice parameter and the lower resolution of EDD measurements.[33] The $d1$ and $d3$ periodicities are the same those observed in the AR-XRD results. The diffraction peak at $q_z = 0.250$ Å^{-1}, marked with a circle, disappears at 83 °C, and is related with the d1 periodicity. Only the tilted $d3 = 34$ Å bilayers (peak at $q_z = 0.185$ Å^{-1}) configuration marked with a triangle – remain up to 98 °C. At higher temperatures, we observe a reflectivity profile evidencing a residual layer on the substrate, with a thickness of ~48 Å, related with the existence of a single bilayer on the substrate.

EDD measurements of OcPA multilayers are shown in Figure 4(b). Two temperature steps were used: from 45 to 75 °C, we performed steps of 0.8 °C and from 75 to 100 °C steps of 0.1 °C were taken, adding up to a total of 312 acquisitions. Only selected curves are shown. Since OcPA alkyl chains are shorter, we have chosen a scattering condition fixed at $\theta = 3.5°$, $2\theta = 7°$, to increase the observed reciprocal space range. Acquisition times of 50 s per temperature were used (with thermalization intervals of 60 s). The periodicities referring to OcPA data are presented in the Table 2. Again, three different configurations are observed at room temperature, in agreement with AR-XRD measurements. The diffraction peak at $q_z = 0.586$ Å^{-1} (identified by a solid triangle) is related to the d3 periodicity and is not observed for temperatures higher than 84 °C. Peaks from the other two periodicities remain up to higher temperatures. The peak at $q_z = 0.485$ Å^{-1}, marked with a circle, is related to the straight bilayer periodicity $d1 = 25.9$ Å and the

dx.doi.org/10.1021/la303087t | Langmuir XXXX, XXX, XXX–XXX

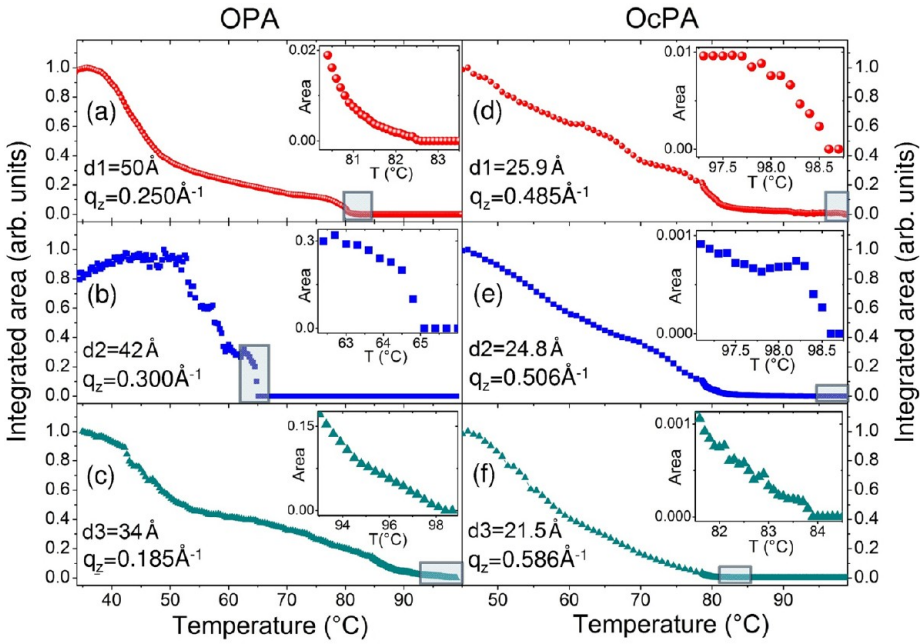

Figure 5. Peak relative integrated area as a function of the temperature for the different OPA bilayer stack configurations: (a) $d1$, straight; (b) $d2$, tilted by an angle of 33°; and (c) $d3$, tilted by 47° with respect to the surface normal. Peak relative areas obtained for OcPA bilayer stack configurations: (d) $d1$, straight; (e) $d2$, tilted by an angle of 17°; and (f) $d3$, tilted by 34°. The insets show details of the order−disorder transition temperatures.

peak at q_z = 0.506 Å^{-1}, marked with a square, is related to the $d2$ = 24.8 Å tilted configuration. At around 98.5 °C, we observed the order−disorder transition of OcPA, and after this temperature no ordered multilayer diffraction signal is detected from the sample. Since the OcPA molecule is shorter, leading to smaller lamellar bilayer periodicity and consequently more spaced diffraction peaks, one can distinguish the $d1$ and $d2$ configurations in OcPA (although they have only 1.1 Å difference).

The analysis of the area below the EDD diffraction peaks gives information about the evolution of the relative volume of each configuration. The areas of the peaks marked with solid symbols in Figure 4 are shown in Figure 5 for bilayer stack configurations from both acids as a function of the temperature. The same analysis process was applied to the peaks marked with open symbols for each molecule multilayer, leading to very similar curves and identical order−disorder temperatures. All areas are normalized by the maximum area of the chosen peak and the analysis is provided relatively to each configuration. Peak areas for the different periodicities of OPA multilayers are presented in Figure 5, parts (a−c). The sample degradation was monitored by exposing a sample at room temperature for long time intervals and used to correct the EDD data.[21] Such procedure reassures that any change in the integrated area curve is due the modifications in the observed stacking sample configuration. In this work, no degradation was observed at OPA and OcPA samples.[34]

Figure 5(a) shows the integrated area for a diffraction peak related to $d1$ = 50 Å, marked with a circle in Figure 4(a). One observes that as the temperature increases, the relative volume of this configuration decreases smoothly, with a hump around 65 °C. In the inset, we show in detail the behavior close to the order−disorder temperature, T_{1c} = 83.1 °C. The normalized area of the peak analyzed for $d2$ = 42 Å [identified by a square in Figure 4(a)] is shown in the Figure 5(b). The relative volume of this tilted configuration extremely reduced compared to the other periodicities (10x less than $d3$ relative volume), and presents a more abrupt transition near 65 °C. The inset shows the critical temperature behavior, near T_{2c} = 65.1 °C.

Finally, the area of the diffraction peak for OPA marked with a triangle, related to the $d3$ = 34 Å tilted bilayer, is presented in the Figure 5(c). The relative volume of this configuration also decreases smoothly and monotonically with the temperature increase. The inset shows in detail the peak area near the order−disorder temperature and the phase transition occurs near T_{3c} = 98.3 °C. After this temperature, no lamellar order is observed in the system. Since OPA molecules acquire enough thermal energy to seek for a more stable configuration as temperature increases, this result evidence that the $d3$ (34 Å) configuration is energetically more stable with respect to $d1$ and $d2$.

Similar analyses were performed on OcPA multilayers. The reduced data sets are shown in Figure 5, parts (d−f). The area of the diffraction peak of periodicity $d1$ [marked with a circle Figure 4(b)] is shown in the Figure 5(d). The order−disorder transition takes place at T_{1c} = 98.6 °C, as depicted in the inset. In Figure 5(e), the evolution of relative volume of the periodicity $d2$ is shown, with the order−disorder temperature (inset) also found at T_{2c} = 98.6 °C. The integrated area of diffraction peak corresponding to the OcPA periodicity $d3$ is presented in the Figure 5(f), with the critical temperature (inset) at T_{3c} = 83.9 °C. We observe for all peaks a smooth decrease of ordered volume as the temperature raises. This can be an indication that molecules are not densely packed inside lamellar layers, with enough space for increasing disorder while temperature is increased.

EDD measurements as a function of the temperature provided information about the modifications in the lamellar packing to OPA and OcPA multilayers. However, such transitions may also be related to modifications in the in-

dx.doi.org/10.1021/la303087t | Langmuir XXXX, XXX, XXX−XXX

plane order, and it is necessary to investigate its thermal evolution. In-plane information can be retrieved by X-ray transmission measurements, most notably SAXS and WAXS. With SAXS measurements, it is possible to observe the existence of large molecules packing such as micelles while WAXS measurements allows one to obtain information about the planar order of molecules.

The planar packing can be determined by the peak sequence on the WAXS scattering patterns. In the case of cubic packing the q positions occur in integer multiples of the first peak, while for hexagonal packing the sequence of peaks follows the rule 1: $2^{1/2}$: $3^{1/2}$: 2: $5^{1/2}$: $6^{1/2}$.[35] WAXS measurements ranging from q_{min} = 1.20 Å^{-1} to q_{max} = 3.10 Å^{-1} were performed as a function of temperature for OPA and OcPa multilayers. Temperature steps of 5 °C were used up to 65 °C while measurements with 2.5 °C step were acquired up to 120 °C. In Figure 6(a), we

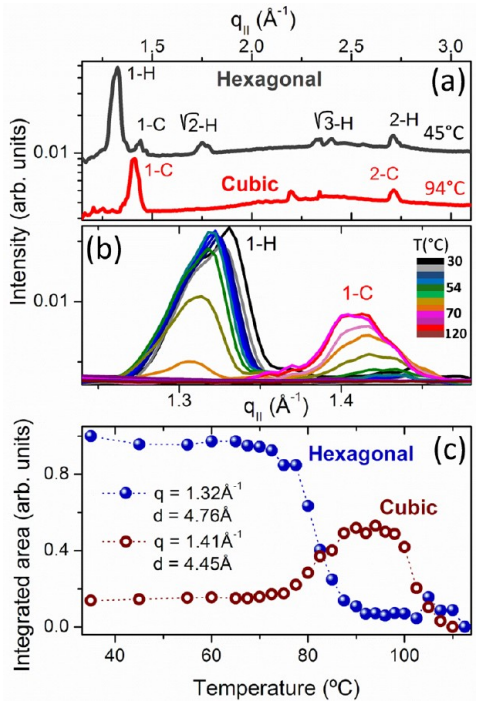

Figure 6. In-plane configuration from OPA multilayers measured by a wide-angle X-ray scattering (WAXS). (a) WAXS measurements indicating hexagonal and cubic packing for OPA at 45 °C (upper curve) and 94 °C (lower curve), respectively. (b) Evolution of the first diffraction peaks observed in (a) as a function of the temperature, showing the change of the in-plane configuration. (c) Normalized integrated peak areas for the peaks shown in (b), evidencing the transition from hexagonal to cubic packing around 83 °C.

show WAXS measurements from OPA multilayers at two selected temperatures. The peaks in the upper curve, measured at 45 °C, follow the q sequence ascribed to hexagonal in-plane packing. At 94 °C, peaks are positioned at integer multiples of the first peak evidencing cubic in-plane packing.

Figure 6(b) shows WAXS measurements for several temperatures depicting the two main peaks at q = 1.32 Å^{-1} and q = 1.41 Å^{-1}. At low temperatures, we observe an intense first peak indicating that most of the molecules are packed hexagonally. As the temperature increases, the peak configuration changes, with a reduction of the first hexagonal packing peak intensity and the rising of the cubic peak intensity. For high temperatures (T > 80 °C), the peak related to cubic packing becomes more significant. By evaluating the area below the two peaks shown in Figure 6(c)—normalized by the maximum area observed in Figure 6(b) − we can follow the modifications in the planar order of OPA molecules as a function of temperature. At lower temperatures, the OPA molecules are ordered in hexagonal packing with d_{hex} = 4.76 Å with a small population of cubic packing. At ∼83 °C, the transition to cubic packing takes place. Between 75 and 85 °C a coexistence of the two in-plane structures is observed. At higher temperatures, the cubic packing prevails with d_{cubic} = 4.45 Å, remaining up to 110 °C. At this latter temperature, the order−disorder transition to OPA molecules in-plane takes place, indicating that intralamellar order survives stacking disorder up to slightly higher temperatures.[36] The SAXS measurements do not show the formation of micelles or any other arrangement in the nm-scale of OPA molecules for all temperatures studied, including temperatures after the order−disorder transition.

Similar measurements were performed in OcPA multilayers to obtain the in-plane configuration, but no well-defined in-plane structure was observed. The interactions of OcPA carbonic chains is reduced compared to OPA molecules, and may result in less organized in-plane configurations,[16] leading to smaller in-plane domains and consequently loss of in-plane registry along the surface perpendicular direction, finally suppressing long-range in-plane organization.

DISCUSSION

The gathered information concerning lamellar and in-plane order allows us to construct a relative configuration phase diagram, showing the normalized (to the unity) ordered fraction of all OPA and OcPA configurations as function of the temperature. In order to produce this phase diagram, several samples containing multilayers of each phosphonic acid studied here were measured by EDD. It was found that while absolute volumes of each ordered configuration vary from sample to sample, phase diagrams of the relative volume (considering the sum of all ordered material volume as unity) are very similar for all studied samples. In order to provide the relative volume, α_n coefficients obtained from eq 1 for AR-XRD fits were used as initial references for peak intensities in the EDD measurements at room temperature and at 60 °C. The excellent agreement between normalized peak areas extracted from both methods using this procedure allowed us to estimate relative volumes with good precision even for phases that were not present in the AR-XRD (like OPA-d2).

The OPA relative volume phase diagram is shown in the Figure 7(a). At low temperatures, one observes the coexistence of three lamellar periodicities and in-plane hexagonal packing. The ordered fraction of each OPA phase changes as the temperature rises. The 42 Å is the periodicity with smaller relative volume fraction, and its representation in Figure 7(a) was amplified by a factor of 5 for better visualization. This is most probably a metastable phase that disappears already at 65.1 °C. The volume fraction of ordered molecules with 50 Å periodicity is dominant at lower temperatures and severely drops after 75 °C, disappearing at 83.1 °C. Such transition coincides with the in-plane transition from hexagonal to cubic packing, indicated by vertical dashed lines in Figure 7(a). In the region between the dashed lines, hexagonal and cubic in-plane packing coexist. At higher temperatures, only 34 Å tilted bilayers still exhibit lamellar order in the system, until the order−disorder temperature of 98.3 °C is reached (after this

dx.doi.org/10.1021/la303087t | Langmuir XXXX, XXX, XXX−XXX

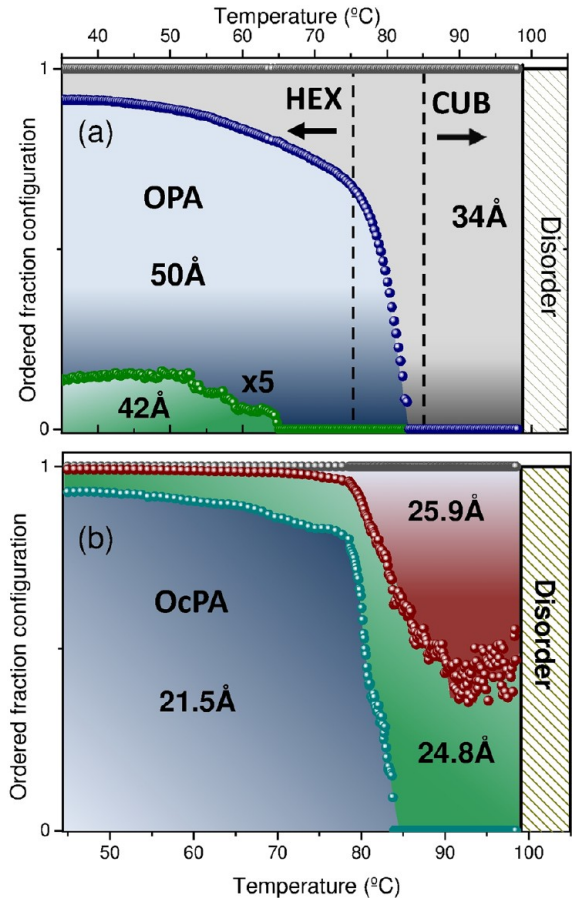

Figure 7. (a) Phase diagram for OPA multilayers showing the lamellar and in-plane configurations as functions of the temperature. The ordered fraction of 42 Å configuration was multiplied by 5 for better visualization. (b) Phase diagram for OcPA multilayers.

temperature the system is disordered in the out-of-plane direction).

The 34 Å configuration remains ordered up to higher temperatures most probably due to an interlock of CH_2 groups in the OPA molecule tails.[13,16,37] This interlock possibility was investigated by Barrena and co-workers[37] in alkylsilane monolayers. Such phenomenon can take place in self-assembled systems of molecules with long zigzag chains composed by CH_2 groups, where the alignment of neighbor chains allow for increasing the molecule density while leading to an overall favorable energy state due to the optimization of van der Waals interactions. The DFT calculations shown in this section corroborate that interlock takes place in our phosphonic acid multilayers.

The relative phase diagram to OcPA multilayers is shown in Figure 7(b). At low temperatures it is possible to observe the coexistence of three periodicities with distinct ordered fraction. The 21.5 Å configuration is the dominant fraction for lower temperatures, disappearing totally at 83.9 °C after decaying along a 5 °C interval. This interval is narrower than the temperature transition interval between 50 and 34 Å bilayers in the OPA multilayers and may indicate a weaker molecular interaction in OcPA low temperature ordered phases. The other two configurations remain at higher temperatures. Significantly larger ordered fractions of 24.8 and 25.9 Å periodicities are observed from 82 °C up to 98.6 °C. Although the straight bilayer is in extreme minority at low temperatures, it becomes dominant for temperatures higher than 85 °C. In OcPA bilayers, the more stable configuration of periodicities with small or zero tilt angles—$d1$ and $d2$ from Table 2—occur probably due to the larger significance of head−head interaction with respect to OPA. Since OcPA molecules have shorter alkyl chains, strongly tilted packing—that could bring interlock of carbonic chains—is unfavored with respect to ordered configurations where adjacent molecule heads can bond, meaning a smaller tilt angle with respect to the surface normal.

The temperature dependence depicted in the phase diagrams obtained for our phosphonic acids can be compared to results available in the literature for fatty acids. These latter lamellar phase transitions are known to depend on the length of the hydrocarbon chain, with larger molecules exhibiting higher phase transition temperatures.[38,39] This is an indication of larger stability of longer molecules, which is also observed here for OPA, where in-plane and out-of-plane order were found to be correlated. Although it has been shown that phosphonic acids can achieve functional configurations that are similar to those observed for fatty acids (see, for example, ref 40 variations of thermal properties can be induced by replacing the headgroup (for a review, see ref 11) leading to scenarios where the behavior of fatty acid molecules with two alkyl chains would significantly differ from the behavior of molecules with a single alkyl chain. Therefore, comparing the thermal stability of fatty acids and phosphonic acids may not be straightforward.

In order to corroborate the energetic stability of the molecular structures retrieved by the experiments, we have performed first principles calculations in both systems (OPA and OcPA). In DFT analysis, we considered OPA molecules in hexagonal and cubic in-plane arrangements. Since we employ periodic boundary conditions, the unit cells that represent each bulk phase contain two molecules, one on top of the other and interacting through the phosphonic ends. The results of the geometry relaxations are shown in Figure 8, parts (a) and (b), respectively. In the hexagonal phase, following the experimental results, the initial geometry was built with the molecules aligned in the vertical direction (straight configuration), whereas in the cubic case, we considered an initial tilt angle of 47° with respect to the surface normal.

In general lines, the optimization of the packing geometry is guided by the attempt to form hydrogen bonds between the heads while the weaker van der Waals interactions, which are taken into account in our DFT implementation, are responsible for orienting the CH_2 groups relative to each other. This leads to the so-called interlock mechanism,[37] which is clearly seen in Figure 8, parts (a−d). We found that the configuration that best reconciles these two interactions is the tilted cubic phase, more stable by 0.24 eV with respect to the straight hexagonal phase. This is in agreement with the experimental data, which indicate that this is the phase which prevails at higher temperatures. Interestingly, the calculations allow us to compare the energetic stability of two tilted cubic configurations. In the first, shown in Figure 8(b), the supercells were built with two aligned molecules oriented in the given tilted angle relative to the horizontal; in the second (called here V-tilted), the tilt angle defines the relative orientation of the two molecules in the supercell, as shown in Figure 8(c). Our calculations indicate that the tilted geometry shown in Figure 8(b) is more stable by 0.21 eV. Detailed views of the tail−tail configuration are shown in the insets of Figure 8, parts (a)−(c).

dx.doi.org/10.1021/la303087t | *Langmuir* XXXX, XXX, XXX−XXX

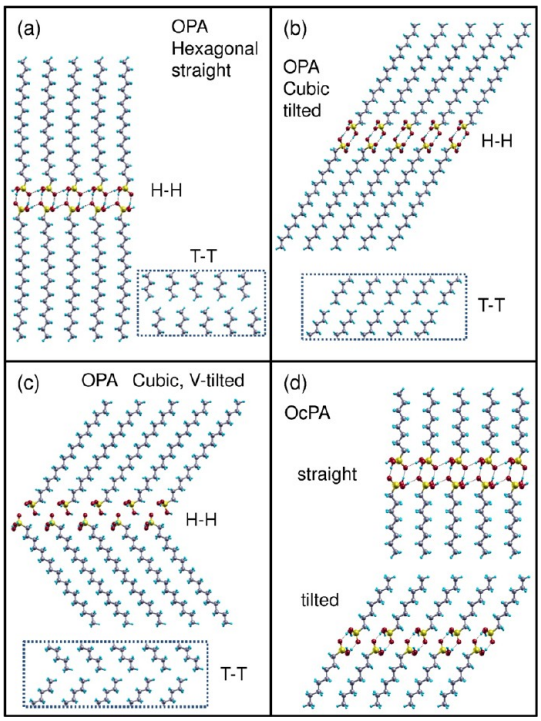

Figure 8. DFT ordering analysis to OPA e OcPA molecule multilayers. The head−head configurations (H−H) are shown in the main figures while detailed tail−tail (T−T) configurations are observed in the insets of parts (a−c). The results of the geometry relaxations are depicted in (a) hexagonal-straight packing and (b) tilted-cubic packing to OPA molecules. (c) Comparison between configurations of V-tilted aligned OPA molecule multilayers that were found to be energetically less favorable than the configuration shown in (b). (d) Simulated relaxed structures of OcPA molecule multilayers, selected among the set of performed calculations.

Similar DFT calculations were conducted for the configurations observed at the OcPA molecule multilayers. Two examples of relaxed structures employed are given in Figure 8(d). We found that for any in-plane configuration, cubic or hexagonal [only the hexagonal geometry is shown in Figure 8(d)], the straight configurations are more stable than the tilted ones, in agreement with the experimental observation which indicates that arrangements with periodicity $d1$ = 25.9 Å are those which survive at higher temperatures. In fact, the geometries that were investigated suggest that vertical orientations optimize the energy due to a compromise between keeping at the same time the favorable head−head hydrogen bond interactions (that are maximized in this orientation with respect to the tilted case) and a fair interlock mechanism at the tails for these smaller molecules.

CONCLUSIONS

In this work, we have schematically depicted the transitions in lamellar and in-plane order of OPA and OcPA molecules as a function of the temperature. It was shown that the molecular length strongly influences the more stable packing configurations and their thermal evolution. For the longer OPA molecules, it was found that the in-plane phase transition from hexagonal to cubic is related to the transition from straight to tilted bilayer lamellar order. The energy differences for the main packing configurations in both multilayer systems were estimated from DFT calculations. Our results point out to a competition of van der Waals interactions and hydrogen bonds in the phosphonic acid multilayer systems. The van der Waals interaction is optimized in the long molecules by tilted states with interlock (OPA case) still with the presence of hydrogen bonds formed at the phosphonic heads. For short molecules (OcPA case), the hydrogen bonds can be maximized and overcome the tail−tail interactions for straight packing configurations.

Since in few-layer systems, the final configuration of molecules can depend on the competition of molecule−molecule and molecule−substrate interactions, the knowledge of the bulk states shown here is crucial to depict whether interactions with the substrate lead to a given final configuration state that is achieved. The results discussed in the text can also be useful for tailoring multilayer systems into a specific configuration for the case of phosphonic acids. One can, for instance, take the system into a temperature where a desired molecular conformation exists and other configurations are in the minority or had vanished and try to stabilize it after quenching the sample (with or without an electric or magnetic field). Such an ability is crucial for fabrication of devices that require controlled coverage and well-defined molecular order to achieve expected performances.

AUTHOR INFORMATION

Corresponding Author

*E-mail: angeloms@fisica.ufmg.br.

Notes

The authors declare no competing financial interest.

ACKNOWLEDGMENTS

The authors thank FAPESP Project 2009/11875-2 and CNPq for financial support. This work was supported by the LNLS under proposals XRF-9851, SAXS-10714, and XRD1-13518. We thank Harry Westfahl and Mateus Cardoso for the support during WAXS/SAXS measurements.

REFERENCES

(1) Su, R.; Liu, H.; Kong, T.; Song, Q.; Li, N.; Jin, G.; Cheng, G. Tuning Surface Wettability of $In_xGa_{(1-x)}N$ Nanotip Arrays by Phosphonic Acid Modification and Photoillumination. *Langmuir* **2011**, *27*, 13220−13225.

(2) Denayer, J.; Delhalle, J.; Mekhalif, Z. Stability of Self-Assembled Monolayers of Organothiol Mono and Bipode on Copper in Presence of Another Organothiol Solution. *Thin Solid Films* **2012**, *520*, 2017−2021.

(3) Yan, C.; Zharnikov, M.; Gölzhäuser, A.; Grunze, M. Preparation and Characterization of Self-Assembled Monolayers on Indium Tin Oxide. *Langmuir* **2000**, *16*, 6208−6215.

(4) Nie, H.-Y.; McIntyre, N. S.; Lau, W. M.; Feng, J. M. Optical Properties of Octadecylphosphonic Acid Self-Assembled Monolayer on a Silicon Wafer. *Thin Solid Films* **2008**, *517*, 814−818.

(5) Klauk, H. Organic Thin-Film Transistors. *Chem. Soc. Rev.* **2010**, *39*, 2643−2666.

(6) Chueh, C.-C.; Higashihara, T.; Tsai, J.-H.; Ueda, M.; Chen., W.-C. All-Conjugated Diblock Copolymer of Poly(3-Hexylthiophene)-Block-Poly(3-Phenoxymethylthiophene) for Field-Effect Transistor and Photovoltaic Applications. *Org. Electron.* **2009**, *10*, 1541−1548.

(7) Tokudome, Y.; Fukushima, T.; Goto, A.; Kaji, H. Enhanced Hole Injection in Organic Light-Emitting Diodes by Optimized Synthesis of Self-Assembled Monolayer. *Org. Electron.* **2011**, *12*, 1600−1605.

(8) Nie, H.-Y.; Miller, D. J.; Francis, J. T.; Walzak, M. J.; McIntyre, N. S. Robust Self-Assembled Octadecylphosphonic Acid Monolayers on a Mica Substrate. *Langmuir* **2005**, *21*, 2773−2778.

(9) Francis, J. T.; Nie, H.-Y.; McIntyre, N. S. ToF−SIMS Investigation of Octadecylphosphonic Acid Monolayers on a Mica Substrate. *Langmuir* **2006**, *22*, 9244−9250.
(10) Dubey, M.; Weidner, T.; Gamble, L. J.; Castner, D. G. Structure and Order of Phosphonic Acid-Based Self-Assembled Monolayers on Si(100). *Langmuir* **2010**, *26*, 14747−14754.
(11) Kaganer, V. M.; Möhwald, H.; Dutta, P. Structure and Phase Transitions in Langmuir Monolayers. *Rev. Mod. Phys.* **1999**, *71*, 779−819.
(12) Bhattacharya, M.; Mukhopadhyay, M. K.; Pal, S.; Sanyal, M. K. Energy Dispersive X-ray Reflectivity to Study Phase Transitions in Thin Films. *Radiat. Phys. Chem.* **2004**, *70*, 611−617.
(13) Fontes, G. N.; Malachias, A.; Paniago, R. M.; Neves, B. R. A. Structural Investigations of Octadecylphosphonic Acid Multilayers. *Langmuir* **2003**, *19*, 3345−3349.
(14) Osman, M. A; Ernst, M.; Meier, B. H.; Suter, U. W. Structure and Molecular Dynamics of Alkane Monolayers Self-Assembled on Mica Platelets. *J. Phys. Chem. B* **2002**, *106*, 653−662.
(15) Klein, R. J.; Fischer, D. A.; Lenhart, J. L. Thermal and Mechanical Aging of Self-Assembled Monolayers as Studied by Near Edge X-ray Absorption Fine Structure. *Langmuir* **2011**, *27*, 12423−12433.
(16) Spori, D. M.; Venkataraman, N. V.; Tosatti, S. G. P.; Durmaz, F.; Spencer, N. D.; Zürcher, S. Influence of Alkyl Chain Length on Phosphate Self-Assembled Monolayers. *Langmuir* **2007**, *23*, 8053−8060.
(17) Neves, B. R. A.; Salmon, M. E.; Russell, P. E.; Troughton, E. B., Jr Spread Coating of OPA on Mica: From Multilayers to Self-Assembled Monolayers. *Langmuir* **2001**, *17*, 8193−8198.
(18) Fontes, G. N.; Moreira, R. L.; Neves, B. R. A. Thermally Induced Stacking of Octadecylphosphonic Acid Self-Assembled Bilayers. *Nanotechnology* **2004**, *15*, 682−686.
(19) Pietsch, U.; Holy, V.; Baumbach, T. *High-Resolution X-ray Scattering: From Thin Films to Lateral Nanostructures*; Springer-Verlag: New York, 2004.
(20) Bodenthin, Y.; Grenzer, J.; Lauter, R.; Pietsch, U.; Lehmann, P.; Kurth, D. G.; Möhwald, H. Temperature- and Time-Resolved X-ray Scattering at Thin Organic Films. *J. Synchrotron Radiat.* **2002**, *9*, 206−209.
(21) Pauli, M.; Pérez, C. A.; Prado, M. C.; Araújo, D. H; Neves, B. R. A.; Malachias, A. Energy Dispersive X-ray Reflectivity Applied to the Study of Thermal Stability of Self-Assembled Organic Multilayers: Results on Phosphonic Acids. *Synth. Met.* **2012**, *161*, 2521−2525.
(22) O'Hare, D.; Evans, J. S. O.; Fogg, A.; O'Brien, S. Time-Resolved, In Situ X-Ray Diffraction Studies of Intercalation in Lamellar Hosts. *Polyhedron* **2000**, *19*, 297−305.
(23) Nie, H.-Y.; Walzak, M. J.; McIntyre, N. S. Bilayer and Odd-Numbered Multilayers of Octadecylphosphonic Acid Formed on a Si Substrate Studied by Atomic Force Microscopy. *Langmuir* **2002**, *18*, 2955−2958.
(24) Hammersley, A. P. *ESRF Internal Report, ESRF97HA02T, FIT2D: An Introduction and Overview*; 1997 Hammersley, A. P.; Svensson, S. O.; Hanfland, M.; Fitch, A. N.; Häusermann, D. Two-Dimensional Detector Software: From Real Detector to Idealised Image or Two-Theta Scan. *High Pressure Res.* **1996**, *14*, 235−248.
(25) Hohenberg, P.; Kohn, W. Inhomogeneous Electron Gas. *Phys. Rev.* **1964**, *136*, B864−B871.
(26) Kohn, W.; Sham, L. Self-Consistent Equations Including Exchange and Correlation Effects. *J. Phys. Rev.* **1965**, *140*, A1133−A1138.
(27) Soler, J. M.; et al. The SIESTA Method for Ab Initio Order-N Materials Simulation. *J. Phys.: Condens. Matter* **2002**, *14*, 2745−79.
(28) Dion, M.; Rydberg, H.; Schroder, E.; Langreth, C.; Lundqvist, B. I. Van der Waals Density Functional for General Geometries. *Phys. Rev. Lett.* **2004**, *92*, 246401−246404.
(29) Román-Pérez, G.; Soler, J. M. Efficient Implementation of a van der Waals Density Functional: Application to Double-Wall Carbon Nanotubes. *Phys. Rev. Lett.* **2009**, *103*, 096102−096105.
(30) Troullier, N.; Martins, J. L. Efficient Pseudopotentials for Plane-Wave Calculations. *Phys. Rev. B* **1991**, *43*, 1993−2006.
(31) Kleinman, L.; Bylander, D. M. Efficacious Form for Model Pseudopotentials. *Phys. Rev. Lett.* **1982**, *48*, 1425−1428.
(32) Als-Nielsen, J.; MacMorrow, D. *Elements of Modern X-ray Physics*; Wiley: Chichester, 2001.
(33) The volume of the periodicity 48.9Å (d2) retrieved from AR-XRD was very reduced, with volume fraction $\alpha_2 = 0.003$, much smaller than the $\alpha_1 = 0.7$ obtained for d_1 =50Å. Hence, although in the EDD analysis, the area of the 50 Å periodicity also includes a contribution from the AR-XRD d2 periodicity, it represents an extremely small addition to the evaluated areas.
(34) In reference 21, we schematically depict the work with energy dispersive diffraction on OPA samples. In this case, the sample exhibited a strong degradation most probably due to insufficient drying time, leading to intralamellar deposits of solvent or water. The preparation procedure for EDD in the samples studied in the present work was significantly improved—using larger drying times and smaller droplets during substrate coating—suppressing the degradation previously effects observed.
(35) Narayanan, T. *Soft Matter: Scattering, Imaging and Manipulation*; Springer-Verlag: New York, 2008.
(36) Cavalcanti, L. P.; Torriani, I. L. Thermotropic Phase Behavior of DPPC Liposome Systems in the Presence of the Anti-Cancer Agent "Ellipticine". *Eur. Biophys. J.* **2006**, *36*, 67−71.
(37) Barrena, E.; Kopta, S.; Ogletree, D. F.; Charych, D. H.; Salmeron, M. Relationship between Friction and Molecular Structure: Alkylsilane Lubricant Films under Pressure. *Phys. Rev. Lett.* **1999**, *82*, 2880−2883.
(38) Peterson, I. R.; Brzezinski, V.; Kenn, R. M.; Steitz, R. Equivalent States of Amphiphilic Lamellae. *Langmuir* **1992**, *8*, 2995−3002.
(39) Overbeck, G. A.; Hönig, D.; Möbius, D. Visualization of First- And Second-Order Phase Transitions in Eicosanol Monolayers Using Brewster Angle Microscopy. *Langmuir* **1993**, *9*, 555−560.
(40) Fabre, R. M.; Okeyo, G. O.; Talham, D. R. Supported Lipid Bilayers at Skeletonized Surfaces for the Study of Transmembrane Proteins. *Langmuir* **2012**, *28*, 2835−2841.